

Measuring Charged Particle Multiplicity with Early ATLAS Public Data

Gözde Üstün[†], Erol Barut[‡], Erhan Bektaş[‡], V. Erkcan Özcan[‡]

[†]*Yıldız Technical University*, [‡]*Boğaziçi University*

(Dated: 07.10.2016)

We study 100 images of early LHC collisions that were recorded by the ATLAS experiment and made public for outreach purposes, and extract the charged particle multiplicity as a function of momentum for proton-proton collisions at $\sqrt{s} = 7$ TeV. As the collisions we study have already been pre-processed by the ATLAS Collaboration, the tracks are visible, but are available to the public only in the form of low-resolution bitmaps. We employ two separate image processing methods, one based on the industry-standard OpenCV library and C++, another based on self-developed algorithms in Python. We present the transverse momentum and azimuthal angle distributions of the particles obtained through both methods, in agreement with the literature.

I. INTRODUCTION

In 2009, when the Large Hadron Collider (LHC) at CERN started to deliver its first physics-quality proton-proton collisions at a center-of-mass (CoM) energy of $\sqrt{s} = 900$ GeV, the very first measurements by the ALICE, ATLAS and CMS Collaborations were of the charged particle multiplicity [1–3]. The goal of such measurements is to understand the momentum and angle distributions of charged particles that result from the so-called *minimum bias events*, which are mostly inelastic collisions at low momentum transfer between the constituents of the protons. Minimum bias events have been useful in understanding the performance of the detectors, and their detailed Monte Carlo simulations play a role in modelling the background to signals of searched particles, such as the Higgs Boson.

The aim of the present work is to perform this multiplicity measurement with very limited resources and using data made public by the ATLAS Collaboration in the form of digitised pictures of select collisions. Since as early as 2010, the ATLAS Collaboration has been publishing event displays of a fraction of the LHC collisions live from a publicly available website [4]. We captured 100 such event displays in May 2011, during the so-called Run1 of the LHC, with collisions at a CoM energy of $\sqrt{s} = 7$ TeV. The trajectories of the charged particles have been reconstructed from the hits they leave in the ATLAS inner detector and are seen as the tracks in the event displays.

We describe two alternative methods for processing the collision images to identify the tracks and extract their azimuthal angles and transverse momenta. One method attempts to use an external image processing library, while for the other, we develop our own application-specific algorithms. In both cases, only free and open-sourced tools and software are used. The programs we develop are portable and work on multiple operating systems, as the authors had access to different resources. The two methods are independent and set different templates for future educational research projects of similar scope. All the development work has been performed by young researchers with no or very limited programming experience.

II. EVENT DISPLAYS

Our data is in the format of png files with 1152×768 resolution. As seen in the example in Figure 1, each display has three panels. A large square panel (765×765) on the left side shows a projection of the detector transverse to the beam (z) axis. ATLAS uses a right-handed coordinate system, with the $+y$ axis pointing vertically upwards and the $+x$ axis pointing towards the center of LHC ring [5]. The top one of the two smaller panels on the right is a ρ - z projection of the detector (ρ is the radial distance to the z axis), while the bottom panel provides details about the particular event, such as its date and time of collection.

The particles that originate from around the interaction point of the beams at the center of detector spread outward going through the inner detector (ID) first, then enter the calorimeters (green and red concentric shells in the transverse view, with yellow boxes representing energy deposits), and finally those that are not absorbed in the calorimeters go through the muon chambers (blue thin blocks in the displays, with gray bars or red points representing particle hits). The outlines of the ID, which consists of three layers of silicon pixel detectors, four more layers of silicon strip detectors, and about 30 layers of gas straw detectors, are depicted as dark gray regions in the center part of the transverse-view displays. These dark gray outlines are clearly visible only for relatively “empty” events, as for most events, the noise and particle hits in light gray color occupy most of the ID in the transverse view.

The ID is immersed in a 2T magnetic field parallel to the z axis. This magnetic field bends the trajectories of the particles, dependent on the magnitude of their transverse momenta, $P_T = \sqrt{P_x^2 + P_y^2}$. The resulting helical tracks, as reconstructed by the ATLAS software from the ID hits, can be seen as colored circular arcs in the transverse view, and as straight lines in the ρ - z projection. Based on displays with very few tracks, it is possible to deduce that each track is drawn in the same color in the two views, but due to a limited selection of track colors (7 in total), most often it is not possible to unambiguously match the arcs to the straight segments. Because of this, we choose to focus only on the higher-resolution transverse view; forsaking the possibility of measuring the pseudorapidity, η , of the particles for now. (Pseudorapidity is defined as a function of the angle, θ , of the particle with respect to the $+z$ axis: $\eta = -\ln(\tan(\theta/2))$.)

As the event displays do not come with any absolute length scale, it needs to be extracted manually. It is worth noting that various layers of the detector do not appear to be up to the same scale, for instance the outermost muon chambers are much larger than what the displays would imply. In order to make sure that at least the various parts of the ID are on the same scale, we measure the apparent sizes of various structures (like the diameters of the various subdetectors of the ID) in pixel units and compare them with their actual sizes from the literature. All these measurements yield ratios within a couple percent of each other. As the best measurement, we pick that of the outer diameter of the thin superconducting magnet, which appears as a thin dark gray ring between the ID and the calorimeters. The scale we obtain is exactly 256 pixels to 2.56 m, so each pixel is taken to represent 1 cm.

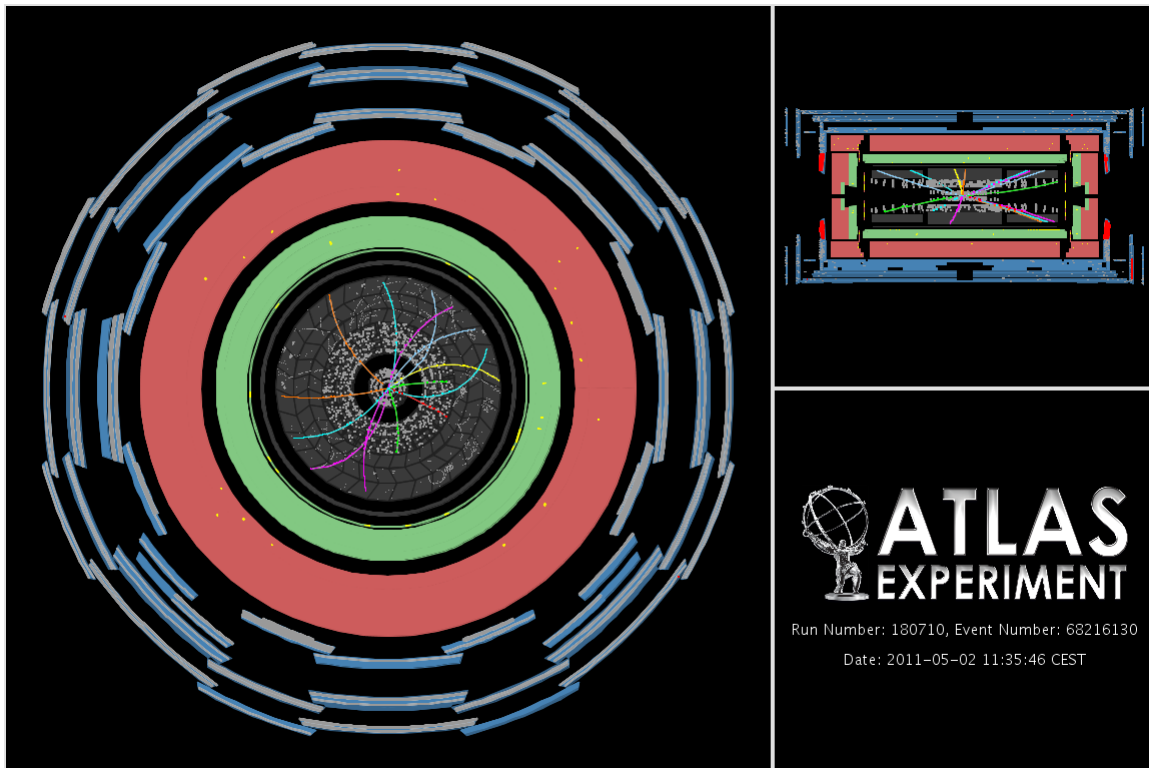


Figure 1. An example event display from our data sample. In the absence of any information to the contrary, we assume that the $+x$ ($+y$) axis is pointing rightward (upward) in the transverse view. This is a low-occupancy event with only 14 tracks.

III. IDENTIFICATION OF TRACK COLORS

Both of our analyses start with a common part: the identification of the distinct colors used for the tracks. For this purpose, we initially remove all the pixels (by painting them black) in the images except those that fall within the transverse view of the ID. Next we identify where in the (R, G, B) colorspace, the seven track colors (red, dark orange, yellow, lime, light sky blue, aqua and fuchsia [6]) and the detector-related gray colors occupy. Towards this goal, we scan the ID part of a few low-occupancy images, and look for clusters in the (R, G, B) space, as seen in the top panels of Figure 2. The gray pixels lie close to the diagonal line between the origin and (255, 255, 255), so in order to remove them, we veto any pixels whose R, G, B coordinates are all within 4 points of each other.

As the seven track colors occupy distinct regions in the (R, G, B) space, we are able to define identification criteria for each of them with relatively high efficiency. We use simple 3D rectangular box cuts (as in the OpenCV's `inRange()` method), with the boundaries chosen in such a way that the selection efficiency of all the colors are within about 10% of each other. The loosest cuts (hence the highest efficiency) are for fuchsia and lime, as they are at two corners away from the other colors, while the tightest cut is for yellow, as its darker hues get gradually similar to orange. The overall efficiency of assigning the non-black, non-gray pixels to any one of the 7 colors is about 69% as measured in the ID regions of all 100 images in our dataset. A significant fraction of the pixels lost during color identification is mainly because of colors getting mixed up around the intersecting tracks. While we note that this fraction will be dependent on the occupancy of the ID, we do not attempt to correct for this systematic effect, as our data consist of relatively-low-occupancy events from the early LHC collisions, when the average collisions per each crossing of the proton bunches was about 7 [7].

Having identified the colors, we look for possible biases in our dataset. Given the cylindrical symmetry of the ATLAS Detector, the tracks are expected to be uniformly distributed over the whole range of azimuthal angles (polar angle in the x - y plane). The bottom right panel of Figure 2 shows the histogram of the azimuthal angle for all the pixels that we identify with any of the 7 colors. We observe a small, but statistically significant bias: the distribution is not really flat, as demonstrated by the very high value of the χ^2 of a straight line fit. We could not identify the cause of this bias; its magnitude and features are partially dependent on color. However it is small enough to be treated as a systematic uncertainty and we derive a correction weight for it at the end of our analyses.

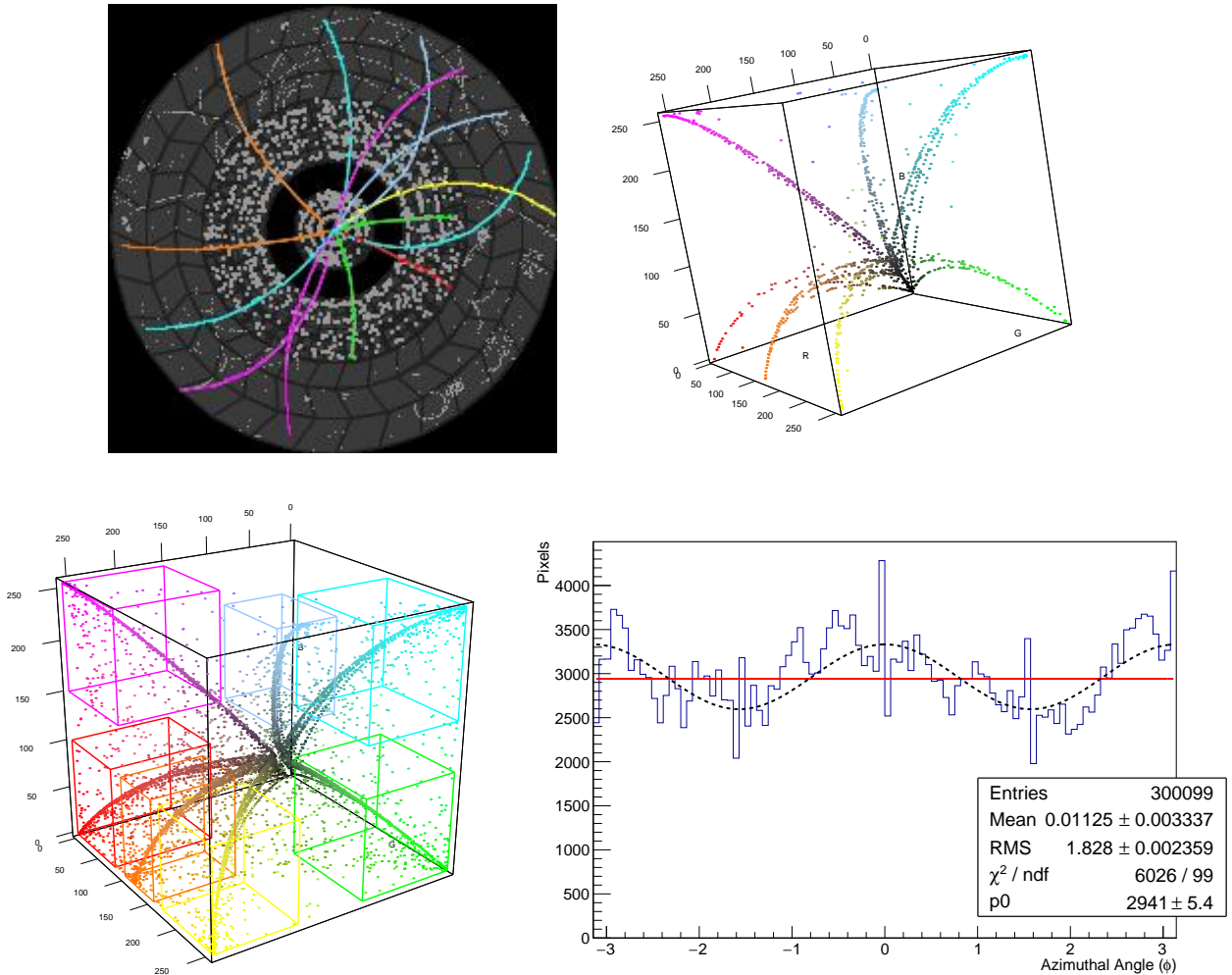


Figure 2. Top left: The ID part of the example event display from Figure 1. Top right: The location in the (R, G, B) colorspace of all the pixels from the top left image. The dark points around the origin (far bottom corner of the cube) are due to the gray color of the ID outline. Seven distinct “threads” can be perceived for each of the colors used for the particle tracks. Bottom left: Colorspace shown for pixels obtained from four high-occupancy events. The gray pixels have been vetoed as described in the text. The colored rectangular prisms demonstrate the selection cuts used to classify the pixels into one of the seven colors. Bottom right: Azimuthal angle distribution of the pixels assigned to any one of the colors. A flat line (red) has been fit to the histogram to check the uniformity of the distribution. Also shown is a fit (black dashed) to a function of the form $\mathcal{N} \times (1 + \alpha \cos(2\phi))$, which describes the distribution better.

IV. ANALYSIS USING A COMPUTER VISION LIBRARY

The first method we utilize to extract information from our data makes use of a freely available computer vision library, OpenCV 2.4.6, which supports hundreds of algorithms for pattern recognition [8]. We chose OpenCV mainly because of its sizeable user community, providing a starting programmer with the avenue of quick online feedback and a large number of code examples. None of the authors had any prior experience with OpenCV or other computer vision libraries. One of the authors, GÜ, tried the C bindings of the library, but we quickly decided that the C++ bindings were more natural and easy to work with. It is worth noting that at this stage, GÜ had no formal training with either C or C++, or any other programming language, beyond some limited tutoring by VEÖ. Our development environment was Orwell Dev-C++ on Windows 8 [9].

For the computer-assisted identification of the tracks, various out-of-the-box techniques from OpenCV were tried. Some of these included connected-component analysis, various generic feature extraction functions such as `goodFeaturesToTrack()`, and the Hough transform (with various degrees of Gaussian smoothing) for extracting circular arcs [10, 11]. Unfortunately these attempts yielded a high rate of mis-reconstructed circles and low efficiency.

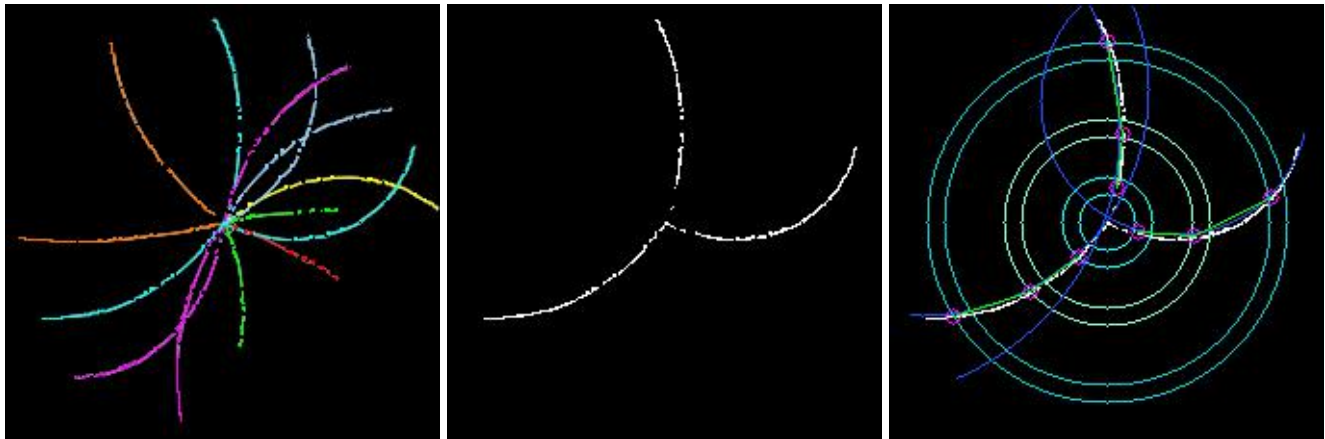


Figure 3. Steps of the “combinatorial” analysis, applied to the example event from Figure 1. Left: Background pixels cleaned. Middle: Pixels of a given color (for example, aqua) selected. Right: Three rings defined; in each ring pixels selected; and from triplets of pixels, tracks reconstructed.

Furthermore, the performance was highly dependent on the detector occupancy. So a decision was taken to implement an algorithm of our own.

As a preparatory step, we wrote a small program with a graphical user interface that allows an end-user to open any image and pick pixels by clicking with a mouse. With each pixel selected, the program prints out its spatial as well as its colorspace coordinates. When a set of three pixels (triplet) is selected, the program solves for the equation of the circle that passes through them, draws the circle and its center on the screen, and prints the calculated P_T .

Our algorithm attempts to automate the manual procedure of picking triplets of same colored pixels. We first split the background-cleaned image into seven subimages, by picking the pixels of each of the identified colors one at a time. On these subimages, we define three 9-pixel-thick concentric rings (of inner radii 15, 45 and 85 pixels, covering parts of the silicon pixel, microstrip and gas straw detectors respectively) and make a list of the colored pixels that fall into them (Figure 3). Whenever two pixels in our list are very close, we choose one randomly. Here we measure the closeness of two pixels as follows: Let \vec{A} and \vec{B} represent the 2D position vectors of the pixels with respect to the center of the ID. Our measure of closeness, which we term “azimuthal distance”, is given by $|\vec{A} \times \vec{B}|/|\vec{A}|$, which is the length of the component of $\vec{B} - \vec{A}$ that is perpendicular to \vec{A} . For pixels in the inner, middle, and outer ring, we require that the azimuthal distance between any two pixels to be at least 6, 8, and 10 pixel sizes, respectively.

With our list of pixels, we try combinations of triplets of pixels, one from each ring, and apply constraints on the locations of the three hits with respect to each other. These constraints are chosen as loosely as possible in order to have a uniform reconstruction efficiency as a function of track P_T . Each pixel from the middle or outer rings is allowed to appear in one triplet only, while pixels from the inner ring can appear in more than one triplet, in order to account for the high occupancy of hits close to the center of the ID. While this decision occasionally generates some partially mis-reconstructed tracks, we find the rate of fakes acceptable in return for higher reconstruction efficiency. Finally, we solve for the equation of the circle for our surviving triplets.

V. ANALYSIS USING APPLICATION-SPECIFIC ALGORITHMS

The goal of our alternative analysis was to perform a detailed pixel-by-pixel processing with completely home-grown algorithms. This would not only serve as a fully-independent cross-check to our OpenCV analysis, but also as a vehicle for testing new algorithm ideas that are specifically tuned for the available data. The work was performed initially with Python 2.6 on Windows, and later with Python 3.4 on Linux and OSX, by two of the authors, EBa and EBe, who had some previous programming experience (but neither had any experience with the advanced features of Python such as classes, iterators, decorators, functional programming, etc.). The code is standard Python with two external dependencies: SciPy 0.13, which is used for least squares optimization, and Pillow 3.3.1, the fork of the lightweight Python Imaging Library (PIL), which is solely used to read the input files and manipulate them pixel by pixel [12–14].

The first algorithm we devise is a clustering algorithm. We start by scanning the ID in search for the pixels that are at the outer endpoints of the circular arcs. Hereafter we use the prefix in- (out-) to describe closer-to (further-away-from) the center of the ID. Hence the outer endpoints of the arcs are pixels of any one of our 7 colors, with no other neighboring pixels of the same color that is further away from the center of the ID. For each outer endpoint found,

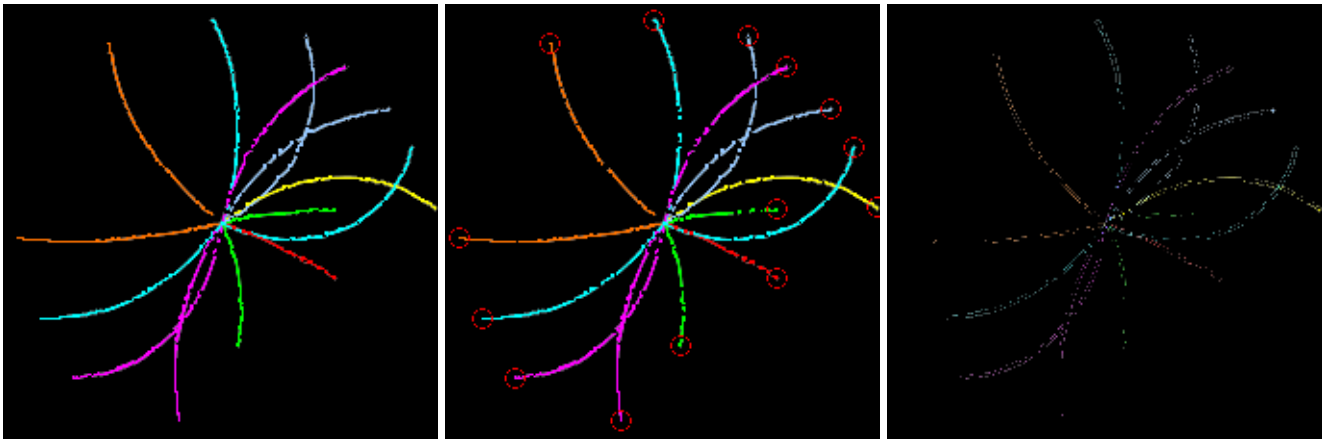


Figure 4. Some of the steps of the “clustering” and “sweeping” analyses being applied to the example event from Figure 1. Left: Outcome of tracklet-merging and filling of the missing parts. Middle: Outer endpoints of the outmost tracklets identified. Right: The unused pixels that were discarded or missed by the sweeping algorithm. They appear as weak shadows of the reconstructed tracks.

we start our outside-in clustering: a tracklet is formed as a set of pixels of a given color, which are inward neighbors of the endpoint or the other pixels in the set. The next step is the merging of tracklets into tracks (Figure 4, left panel). The intersection of different colored tracks or the presence of gray-colored detector hits break the tracks into pieces, which get reconstructed as separate tracklets. We identify the innermost pixel of each tracklet and check if the outer endpoint of another one of the same color is close by. As a final step, we handle incorrectly clustered parts of intersecting tracks of a given color, by searching for kinks in our clusters by examining unexpected jumps in the azimuthal angles of the pixels. For such cases we rerun our clustering algorithm with constraints on the angles. The result is satisfactory for the example event from Figure 1, where we are able to reconstruct all 14 tracks.

Unfortunately, the performance degrades quickly with increased multiplicity of tracks. The tracklet merging and the kink identification have a number of parameters that need careful tuning and we have observed that high occupancy events require highly different tunes. As an alternative solution, we devise a second algorithm, the “sweeping” analysis. From the clustering algorithm, we take the best performing part, outer-endpoint identification, and perform the following steps:

1. Apply endpoint identification to find the outer endpoints of the outmost tracklets (Figure 4, middle panel).
2. For each identified end-point, define a 17-pixel-thick ring that is centered on the endpoint and whose mid-radius is half the distance between the endpoint and the center of the ID. Make a set of “candidate midpoints”: pixels that fall into the ring and whose color is the same as the endpoint.
3. For each midpoint identified in the second step, define a circular arc that connects the endpoint to the center of the ID and passes through the midpoint. Count how many other pixels of the same color are on or within ± 2 pixels around each such arc.
4. Amongst the arcs defined in the third step, pick the one with the highest count of pixels. Perform a least squares fit (details below) to those pixels to extract the precise equation of the arc. From its radius, compute the transverse momentum $P_T[\text{GeV}/c] = B[\text{T}] \times r[\text{m}] \times 0.2998[\text{m/ns}]$ and other parameters of interest. Remove the used pixels from the original image.
5. Repeat steps 2 thru 4 until no tracks are left to be reconstructed, “sweeping out” a very large fraction of all the colored pixels. The few remaining pixels at the end of the whole procedure can barely be perceived in the rightmost panel of Figure 4.
6. On rare occasions, a track gets reconstructed more than once using mutually exclusive subsets of its pixels. To remove the duplicates, search for pairs of reconstructed arcs of the same charge (based on whether they turn clockwise or counterclockwise), of the same color, and whose centers are within 15 pixels of each other. If the associated number of pixels for either of the pair is fewer than 15, or if the measured radii of the pair are within 0.5% of each other, discard the arc with the fewer pixels.

The circle fit we perform in step 4 itself proceeds through two substeps. The first substep has been implemented by one of the authors, EBa, who derived an algebraic solution using basic principles from a linear algebra textbook [15]. This solution looks for values of (x_C, y_C, R) , coordinates of the center and the length of the radius, that minimize $S = \sum_i ((x_i - x_C)^2 + (y_i - y_C)^2 - R^2)^2$, where (x_i, y_i) are the coordinates of the pixels being fit. A later literature search revealed that this minimization is known as Kåsa's method [16]. Unfortunately, a visual inspection quickly reveals that this method systematically underestimates the radius for incomplete circles like the arcs we have in our data. So as a second substep, we proceed to do a full least squares fit that minimizes $S' = \sum_i (\sqrt{(x_i - x_C)^2 + (y_i - y_C)^2} - R)^2$ using numerical methods. For this purpose, `optimize.leastsq()` function from the SciPy library, an implementation of the Levenberg-Marquardt algorithm, is used. We pass the center coordinates computed using Kåsa's method as an initial estimate to the numerical method, in an attempt to improve the speed of the computation.

The final results from the sweeping analysis are shown in Figure 5. Over 3800 tracks have been reconstructed from 98 events with an average number of 77 pixels per track. (Two events in our dataset had significant activity only in the forward muon chambers and no ID tracks.) After a visual inspection of the busiest images (those with over 60 tracks), we conclude that our reconstruction efficiency is close to 100%. (In comparison, the fast combinatorial analysis reconstructs about 60% of those tracks; some lost because they do not reach the gas straw detectors.) The fake rate (tracks mis-reconstructed from unrelated pixels) is harder to estimate accurately; as a substitute we modify some of the critical parameters of our algorithms to see how robust our final results are. The parameter to which the sweeping algorithm is most sensitive appears to be the width of the arc in third step. Doubling (± 4 pixels) this parameter means lumping more hits together and decreases the total number of tracks by about 8%. We believe that assuming a fake rate of about 10% is then reasonable.

The angular distribution of the reconstructed tracks is mostly flat, after taking into account the bias observed in the distribution of the pixels in the dataset. The resolution in the measurement of the transverse impact parameter, i.e. the transverse distance of closest approach to the center of the ID, is determined to be 1.64 cm, higher than our naive expectations. Upon further investigation, we observe that this value is a decreasing function of the number of pixels associated with the tracks, as we would expect, but the relationship is not a simple $\propto N_{pixels}^{-1/2}$ function, suggesting that the pixelation of the images plays an important role: perhaps the actual center of the ID is not really aligned with the center of any given pixel. Such a hypothesis could also provide a partial explanation of the bias in the azimuthal angle distribution of the colored pixels, but our attempts to confirm the hypothesis have failed.

VI. COMPARISON TO PAST MEASUREMENTS

As we do not have the pseudorapidity values of the tracks, a direct comparison to the published ATLAS results from Reference [17] is not possible. However, in that publication it is stated that the ATLAS measurement is compatible with the simulated collisions from the Monte Carlo event generator program Pythia6 after a special tuning of the program's parameters. We use Pythia 6.4.28, with the advised AMBT1 tune to generate 1000 collision events of our own for comparison with our results [18]. Unfortunately such events are not directly comparable either, as the inefficiencies of the ATLAS Detector need to be taken into account.

In order to imitate those inefficiencies, we digitize and extract values from Figure 2(d) of [17] using the open-source program WebPlotDigitizer 3.3 [19]. With another open-source program, ROOT 5.34/24 [20], a 6th-order polynomial is fit to the extracted values in order to obtain an empirical formula describing the detector efficiency as a function of $\log(P_T)$ (Figure 6, left). In the very low P_T region where our empirical function gives negative efficiencies, the efficiency is taken to be zero, while for $P_T > 40$ GeV/c (above the range of the ATLAS plot), we take a constant value of 86.6%. For each charged particle in the Pythia6-generated events, the efficiency corresponding to its P_T can then be computed with our empirical function and applied as a weight while filling the simulation histograms.

The comparison of the simulated charged particle P_T and the results of our sweeping analysis are shown on the right panel of Figure 6. Higher momentum tracks are comparatively more frequent in our data, but the most significant difference is the shortage of tracks below 0.5 GeV/c. We suspect that both of these observations are related to ATLAS's selection of events for public consumption; 0.5 GeV/c could be the side effect of the ATLAS trigger that feeds the data stream used for outreach purposes. In our comparison plot, we have assumed the presence of such a cutoff in determining the normalization of the simulated data. Despite the minor differences mentioned, we find the level of agreement unexpectedly satisfactory.

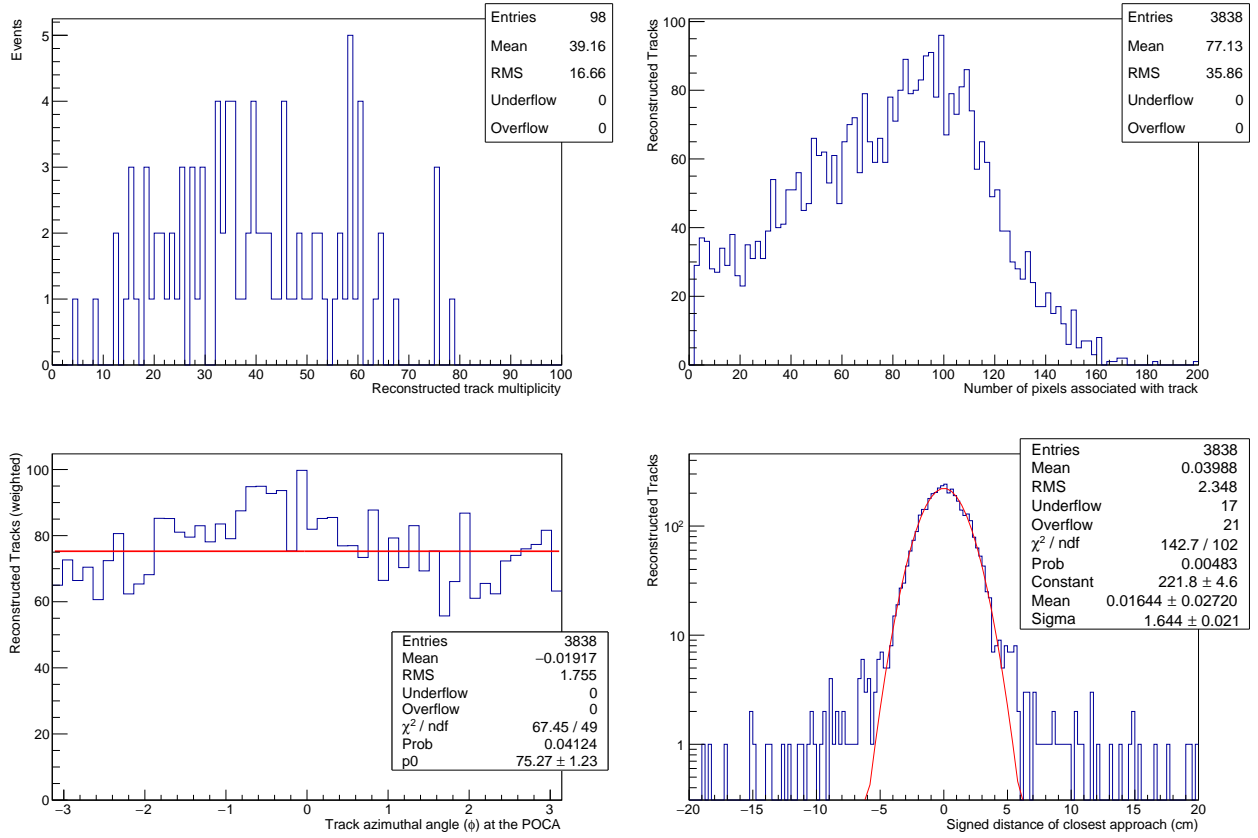


Figure 5. Some results from the “sweeping” analysis. Top left: Track multiplicity per event. Top right: Number of pixels associated with the reconstructed tracks. Bottom left: Azimuthal angle of tracks computed at the point of closest approach to the center of the ID. The histogram is filled with each track assigned a weight given by $(1 + \alpha \cos(2\phi))^{-1}$, where $\alpha = 0.124$, in order to overcome the bias observed in the distribution of the pixels in Figure 2. A flat line fit (in red) is also shown. Bottom right: Distance of closest approach to the center of the ID, multiplied by the charge of the track. A Gaussian function (in red) has been fit to the histogram.

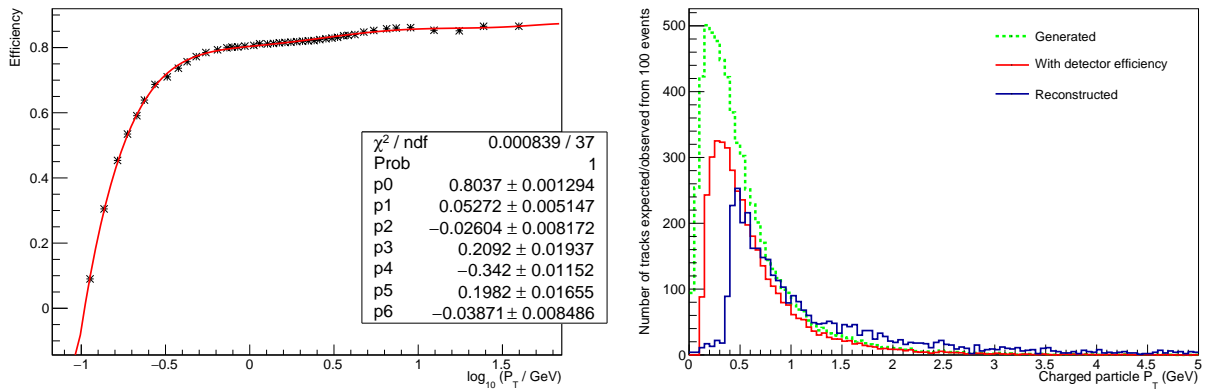


Figure 6. Left: Efficiency of the ATLAS Detector as a function of $\log(P_T)$. Data points (black stars) have been extracted from Reference [17]. The listed parameters p_0, \dots, p_6 are the constants of the fitted polynomial (red curve). Right: Comparison of the charged particle transverse momentum histograms obtained as a result of our reconstruction (blue solid) and from Monte Carlo simulation (red solid). Also shown is the distribution from the MC generator before the P_T -dependent ATLAS detector efficiency corrections have been applied (green dashed).

VII. CONCLUSION

We have shown the feasibility of repeating a cutting-edge measurement, one that was featured as the beginning of “the dawn of exploration of a new energy frontier at the LHC” in a Physics Synopsis by the American Physical Society [21], with the help of freely-available tools being used by young researchers with no or little prior experience. (GÜ was a high school student for most of her work on the OpenCV-based analysis, while EBe and EBa, who devised the clustering and sweeping algorithms were junior and freshman physics majors respectively.) Despite our lack of a full understanding of the detector behaviour, our results are broadly in agreement with the simulated results that have been generated in accordance with the publications by the ATLAS Collaboration.

The two different approaches we have described are complementary and constitute examples of projects of different scopes. The combinatorial analysis is fast (processing 100 events in about 4 minutes on a 2.2 GHz Intel Core i7), utilizes compiled C++ code and an industry-standard computer vision library, and does inside-out tracking. Its logic closely resembles fast trigger tracking codes used by the LHC experiments. The clustering and sweeping analyses are much slower (1 event per minute on average), utilize interpreted Python code and a lightweight image manipulation library, and perform outside-in tracking. It is in the spirit of slow offline tracking algorithms of the LHC experiments, and yields results of high resolution. In spite of the fact that Python is arguably a more expressive language than C++, their code is longer and more complex than that of the combinatorial analysis.

The displays of events we collected in the early days of the 7 TeV running of the LHC has given us a unique opportunity to study the charged particle tracks in the inner detector of the ATLAS Detector. The higher CoM energy and much higher instantaneous luminosity make the possibility of repeating our work difficult with more recent collisions, due to the large amount of particles in the events. However the new fish-eye event displays made public by the ATLAS Experiment show energy deposits in the calorimeters and hits in the muon chambers very distinctly, allowing interested students to share the experience we have outlined in this paper in their own unique ways. In such future studies, it might be possible to measure missing transverse energy, a parameter fundamental in the search for beyond the Standard Model physics.

ACKNOWLEDGMENTS

We would like to thank Deniz Niyazi for her support of GÜ during the middle stages of the project, and Fatih Mercan for providing feedback on our early drafts. VEÖ would like to thank Boğaziçi University Foundation (BÜVAK) and the Science Academy Society of Turkey for their indirect financial support. We are grateful for the access that the LHC experiments provide to their data, in formats that are inspiring for the public.

-
- [1] ALICE Collaboration (K. Aamodt et al.), “First proton–proton collisions at the LHC as observed with the ALICE detector: measurement of the charged-particle pseudorapidity density at $\sqrt{s} = 900$ GeV,” *Eur. Phys. J. C* **65**, 111–125 (2010).
 - [2] ATLAS Collaboration (G. Aad et al.), “Charged-particle multiplicities in pp interactions at $\sqrt{s} = 900$ GeV measured with the ATLAS detector at the LHC,” *Physics Letters B* **688**, 21–42 (2010).
 - [3] CMS Collaboration (V. Khachatryan et al.), “Transverse-momentum and pseudorapidity distributions of charged hadrons in pp collisions at $\sqrt{s} = 0.9$ and 2.36 TeV,” *JHEP* **02** (041), 1–19 (2010).
 - [4] Live Collisions in the ATLAS Detector, <http://atlas-live.cern.ch/public/>
 - [5] ATLAS Collaboration (G. Aad et al.), “The ATLAS experiment at the CERN Large Hadron Collider,” *JINST* **3** S08003, i-407 (2008).
 - [6] We use the names of the closest colors from the CSS3 recommendation by W3C. T. Çelik, C. Lilley, L. D. Baron (ed.), “CSS Color Module Level 3, W3C Recommendation 07 June 2011”, <https://www.w3.org/TR/css3-color/>
 - [7] ATLAS Collaboration, “Luminosity Public Results,” https://twiki.cern.ch/twiki/bin/view/AtlasPublic/LuminosityPublicResults#2011_pp_Collisions
 - [8] Open Source Computer Vision (OpenCV), <http://opencv.org/>
 - [9] Orwell Dev-C++ provides a suite for running gcc on the Windows platform. <http://orwelldevcpp.blogspot.com>
 - [10] Jianbo Shi and Carlo Tomasi, “Good Features to Track,” *Proceedings of the IEEE Conference on Computer Vision and Pattern Recognition*, 593–600 (1994).
 - [11] H.K. Yuen, J. Princen, J. Illingworth, J. Kittler, “Comparative study of Hough Transform methods for circle finding,” *Image and Vision Computing* **8** (1), 71–77 (1990).
 - [12] Eric Jones, Travis Oliphant, Pearu Peterson and others, “SciPy: Open source scientific tools for Python”, <https://www.scipy.org/>
 - [13] Python Imaging Library, PIL, <http://www.pythonware.com/products/pil/>
 - [14] Pillow, The Friendly PIL Fork, <https://python-pillow.org/>

- [15] Gilbert Strang, *Linear algebra and its applications*, 2nd edition (Academic Press, New York, 1980), pp. 111-120.
- [16] I. Kása, “A circle fitting procedure and its error analysis”, IEEE Transactions on Instrumentation and Measurement **25**, 8-14 (1976).
- [17] ATLAS Collaboration (G. Aad et al.), “Charged-particle multiplicities in pp interactions measured with the ATLAS detector at the LHC,” New Journal of Physics **13** 053033, 1-68 (2011).
- [18] Torbjörn Sjöstrand, Stephen Mrenna and Peter Skands, “PYTHIA 6.4 physics and manual,” Journal of High Energy Physics **2006** (05), 026 (2006).
- [19] Ankit Rohatgi, WebPlotDigitizer, <http://arohatgi.info/WebPlotDigitizer/>
- [20] Rene Brun and Fons Rademakers, “ROOT - An Object Oriented Data Analysis Framework,” Proceedings AIHENP'96 Workshop, Lausanne, Sep. 1996, Nucl. Inst. & Meth. in Phys. Res. **A 389**, 81-86 (1997). See also: <http://root.cern.ch/>
- [21] Robert Garisto, “Synopsis: Background checking at LHC,” July 6, 2010, <http://physics.aps.org/synopsis-for/10.1103/PhysRevLett.105.022002>